Hover Control of an UAV With Backstepping Design Including Input Saturations

José Raul Azinheira and Alexandra Moutinho, *Member, IEEE*

***Abstract*—This brief presents a backstepping-based controller with input saturations, applicable for the hover flight of an unmanned aerial vehicle (UAV). A dynamic model for a generic UAV is introduced that is valid for quasi-stationary conditions, with quaternion formulation of the kinematics equations. Based on this model, a backstepping design formulation is deduced for UAV hover control, and its global asymptotic stability is demonstrated. In order to cope with limitations due to reduced actuation, saturations are introduced in the control design, and the stability of the modified control solution is verified. Simulation results are presented for the hover stabilization of an airship UAV, which are demonstrative of the excellent performance of the proposed controller and illustrate its robustness in face of wind disturbances.**

***Index Terms*—Backstepping, input saturations, nonlinear control, stabilization, unmanned aerial vehicle (UAV).**

I. Introduction

UNMANNED aerial vehicles (UAVs) have a wide potential as observation and data acquisition platforms. Inspection-oriented applications cover different areas such as landmine detection,[1] agricultural and livestock studies, crop yield prediction, land use surveys in rural and urban regions, broadband Internet for remote rural areas and moving trains [1], and fire detection [2]. For these types of applications, the UAV must often be able to sustain a quasi-stationary flight state (hover flight) independent of the atmospheric conditions. Different kinds of control techniques have been recently applied to solve the hovering problem for diverse types of UAVs. The automatic hovering of an outdoor autonomous airship using image-based visual servoing in a PD error feedback scheme was presented in [3]. Linear robust multivariable control, fuzzy logic control with evolutionary tuning, and nonlinear tracking control were the three control methodologies compared in [4] for a helicopter autopilot design. Also, for hover control of a helicopter, the work in [5] introduced a preliminary study on the use of neural adaptive control techniques, the authors of [6] investigated the decoupling nonlinear H_∞ control design subject to model parameter uncertainties, and the work in [7] proposed a Lyapunov control design using backstepping techniques for a model helicopter. A robust hovering control of a PVTOL aircraft was proposed in [8] based on an optimal control approach. With the exception of [9], which derived a visual servoing control law for UAV bridge inspection based on the backstepping approach, work done on hover control is usually designed for a determined type of UAV. The purpose of this study is to design a hover controller independent of the application UAV.

For the purpose of position and attitude control, the UAV model must be available, usually comprised of dynamic and kinematic equations. For aerial vehicles, aerodynamic forces play an important role. However, a simplistic assumption neglecting these forces may be taken in hover or forward flight with slow velocity. In these conditions, the relative wind dynamics may practically be negligible, with the consequent loss of authority of any control surface. The dynamics model may then only consider external forces and moments originated from motors of propulsion or rotors. This assumption is taken in several applications with UAVs working in near-hover conditions, like helicopters [4], [7], [10] and robot UAVs [9]. It shall be considered here as well for a generic UAV in quasi-stationary flight.

The separation of the UAV model in dynamic and kinematic equations in a cascaded-systems appearance suggests that the backstepping solution, which is a Lyapunov-based control design approach [11], can be easily applied. By formulating a scalar positive function of the system states and then choosing a control law to make this function decrease, we have the guarantee that the nonlinear control system thus designed will be asymptotically stable. Moreover, it will be robust to some unmatched uncertainties. Backstepping has been successful in several applications of flight control [12]–[14]. Addressing also the issue of underactuated systems, this control technique has been applied in [15] and [16].

In a low airspeed or hovering state, the aerodynamic forces are reduced, and consequently the control surfaces authority, thus demanding a superior action by the motors for position and attitude control. This might lead to saturation of the control signals, which are usually bounded. The key issue is then how to include these input limitations in the controller synthesis. Teel [17] proposed a nonlinear combination of saturation functions of linear feedbacks that globally stabilized a chain of integrators. This approach was applied with backstepping in [18] so the limitation of the control signals and its derivative was propagated through each step of the recursive design and in [9] for an UAV with orientation limits.

This brief introduces a dynamic model for a generic UAV that is valid for quasi-stationary conditions, with quaternion formulation of the kinematic equations. A backstepping design formulation based on this model is then deduced for UAV hover control, and its global asymptotic stability is demonstrated. In order to cope with limitations due to reduced actuation, saturations are introduced in the control design, and the stability of the modified control solution is verified.

The above-mentioned assumption neglecting the aerodynamic forces may be an overtaken consideration for an airship

Manuscript received July 6, 2005; revised November 22, 2006. Manuscript received in final form May 17, 2007. Recommended by Associate Editor D. Schoenwald. This work was supported in part by the Portuguese Ministry of Science/FCT through Grant POSI/SRI/45040/2002 and the European FEDER Program through Project DIVA.

The authors are with IDMEC, Department of Mechanical Engineering, Instituto Superior Técnico, Technical University of Lisbon, 1049-001 Lisbon, Portugal (e-mail: (jraz@dem.ist.utl.pt; moutinho@dem.ist.utl.pt).

Color versions of one or more of the figures in this brief are available online at http://ieeexplore.ieee.org.

Digital Object Identifier 10.1109/TCST.2007.908209

[1][Online]. Available: http://www.MineSeeker.com.

UAV case due to its large volume when compared with that of a helicopter, for instance. For this reason, and to demonstrate the effectiveness and excellent performance of the proposed methodology, simulation results are presented for the hovering stabilization of an airship UAV considering three wind scenarios: no wind, constant wind incidence, and turbulent gust disturbances.

This brief is organized as follows. The modeling and backstepping design are presented in Section II. The definitions of saturations are introduced in Section III, and they are included in the control design in Section IV. Simulation results applying the proposed control solution to an airship UAV are presented in Section V. Finally, Section VI draws some conclusions and introduces the ideas of subsequent work.

II. Model and Control Design

Here, a dynamic model is derived for a generic UAV in near-hover conditions. Afterwards, based on this model, a backstepping controller is designed for UAV stabilization.

A. UAV Dynamics

The dynamics of a UAV may be expressed in the form

$$M\dot{x} = -\Omega_6 M x + E S a_g + f \tag{1}$$

where

- M 6-D symmetric inertia matrix;
- x $= [v^T, \omega^T]^T$—6-D velocity state expressed in the local frame;
- v linear velocity;
- ω angular velocity;
- Ω_6 6-D antisymmetric matrix;
- E 6-D gravity matrix input;
- S transformation matrix from fixed to local frame;
- a_g gravity acceleration in the fixed frame;
- f 6-D force input.

The Ω_6 and E matrices are defined as

$$\Omega_6 = \begin{bmatrix} \Omega_3 & 0 \\ 0 & \Omega_3 \end{bmatrix}; \quad E = \begin{bmatrix} m_w I_3 \\ m C_3 \end{bmatrix} \tag{2}$$

where m is the UAV mass, m_w is its weighting mass or heaviness (difference between the weight and buoyancy forces), I_3 is the identity matrix, and C_3 and Ω_3 are the matrix representation of the cross product

$$\begin{cases} C_3 = c\times \\ \Omega_3 = \omega\times \end{cases} \tag{3}$$

where c represents the coordinates of the center of gravity in the local frame.

A generic UAV model includes forces from propulsion, aerodynamics. and wind in the 6-D force input f. In a near-hover case (low airspeed or hovering state), the aerodynamic and wind forces are reduced or null, and the UAV position and attitude are mainly controlled by the action of motors or rotors. In this scenario, a simplistic assumption considering only the propulsion forces may be taken, as will be the case here.

B. UAV Kinematics

The most widely used method for the kinematics representation is based on an Euler angle description [9], [19], [20]. However, there is an inherent geometric singularity in the Euler representation, that does not reflect any intrinsic characteristic of the UAV dynamics. To avoid artificial singularities due to the attitude representation, [14] operated directly in the configuration manifold of the helicopter. References [6], [12] and [15] used a more global solution by recurring to the quaternions representation [21], a four-parameter description that provides a unique representation of the attitude and does not suffer from the singularity problems of the Euler equations. The quaternions are here chosen for attitude representation with the purpose of obtaining a kinematics model valid for any type of UAV, from helicopters to airships. Also, the quaternions representation allows an easier mathematical manipulation, used for the controller design.

Let the UAV position $\tilde{\eta}$ be described by its Cartesian coordinates $p = [p_N, p_E, p_D]^T$ in the North-East-Down frame and by a quaternion description $q = [q_1, q_2, q_3, q_4]^T$ for its angular attitude. The UAV position error may then be defined as $\eta = \tilde{\eta} - \tilde{\eta}_{\text{ref}}$, where $\tilde{\eta}_{\text{ref}}$ corresponds to a given position reference.

The kinematics involves the transformation between velocity and position [21]

$$\begin{cases} \dot{p} = S^T v \\ \dot{q} = \frac{1}{2} Q \begin{bmatrix} 0 \\ \omega \end{bmatrix} \end{cases} \tag{4}$$

or

$$\dot{\eta} = \begin{bmatrix} S^T & 0_{3,4} \\ 0_{4,3} & \frac{1}{2}Q \end{bmatrix} C x = DCx = Tx \tag{5}$$

where Q is the matrix relating the quaternions with their derivatives and the angular rates

$$Q = \begin{bmatrix} q_0 & -q_1 & -q_2 & -q_3 \\ q_1 & q_0 & -q_3 & q_2 \\ q_2 & q_3 & q_0 & -q_1 \\ q_3 & -q_2 & q_1 & q_0 \end{bmatrix} \tag{6}$$

and $C = \begin{bmatrix} I_3 & 0_3 \\ 0_{1,3} & 0_{1,3} \\ 0_3 & I_3 \end{bmatrix}$ is of size (7,6).

The derivatives of the matrices in D are

$$\dot{S} = -\Omega_3 S \Rightarrow \dot{S}^T = S^T \Omega_3 \tag{7}$$

and

$$\dot{Q} = \frac{1}{2} Q \Omega_4 \tag{8}$$

where Ω_4 is a second antisymmetric matrix associated with the angular velocity $\omega = [\omega_1, \omega_2, \omega_3]^T$ as

$$\Omega_4 = \begin{bmatrix} 0 & -\omega_1 & -\omega_2 & -\omega_3 \\ \omega_1 & 0 & -\omega_3 & \omega_2 \\ \omega_2 & \omega_3 & 0 & -\omega_1 \\ \omega_3 & -\omega_2 & \omega_1 & 0 \end{bmatrix} \tag{9}$$

leading to

$$\dot{D} = \begin{bmatrix} S^T & 0 \\ 0 & \frac{1}{2}Q \end{bmatrix} \begin{bmatrix} \Omega_3 & 0 \\ 0 & \frac{1}{2}\Omega_4 \end{bmatrix} = D\Omega_7. \tag{10}$$

The quaternion matrix Q is unitary, leading to the following property of the T matrix:

$$T^T T = C^T \begin{bmatrix} SS^T & 0 \\ 0 & \frac{1}{4}Q^T Q \end{bmatrix} C = \begin{bmatrix} I_3 & 0 \\ 0 & \frac{1}{4}I_3 \end{bmatrix}. \tag{11}$$

If we define the following diagonal matrices

$$\Delta = \begin{bmatrix} I_3 & 0 \\ 0 & \frac{1}{2}I_3 \end{bmatrix}; \quad \Delta_7 = \begin{bmatrix} I_3 & 0 \\ 0 & \frac{1}{2}I_4 \end{bmatrix} \tag{12}$$

then we get

$$T^T \Delta_7^{-2} T = \Delta^{-2} T^T T = I_6 \tag{13}$$

or two formulations for the left pseudo-inverse of T as

$$T^+ = T^T \Delta_7^{-2} = \Delta^{-2} T^T. \tag{14}$$

These formulations are only achievable due to the fact that the quaternions are used instead of the Euler angles for attitude representation.

C. Backstepping Controller Design

Gathering both the dynamic and kinematic equations leads to the system dynamics

$$\begin{aligned} \dot{x} &= Kx + M^{-1}(ESa_g + f) \\ \dot{\eta} &= DCx \\ \dot{S} &= -\Omega_3 S \\ \dot{D} &= D\Omega_7 \end{aligned} \tag{15}$$

where $K = -M^{-1}\Omega_6 M$ linearly depends on the velocity x, whereas M is constant or slowly varying.

Consider two intermediate output variables

$$\begin{cases} y_1 = a\eta + Tx \\ y_2 = \Delta x \end{cases} \tag{16}$$

where a is a positive scalar, and let us define the tentative Lyapunov function

$$W = \frac{1}{2} y_1^T y_1 + \frac{1}{2} y_2^T y_2. \tag{17}$$

Then, the derivative of W is

$$\dot{W} = y_1^T \dot{y}_1 + y_2^T \dot{y}_2 \tag{18}$$

where

$$\begin{aligned} \dot{y}_1 &= a\dot{\eta} + \dot{T}x + T\dot{x} = aTx + D\Omega_7 Cx + T\dot{x} \\ \dot{y}_2 &= \Delta \dot{x} \end{aligned} \tag{19}$$

leading to

$$y_2^T \dot{y}_2 = (\Delta x)^T \Delta \dot{x} = x^T \Delta^2 \dot{x} = x^T T^T T \dot{x}. \tag{20}$$

Finally

$$\dot{W} = (a\eta + Tx)^T (aTx + D\Omega_7 Cx + T\dot{x}) + (Tx)^T T\dot{x} \tag{21}$$

or

$$\begin{aligned} \dot{W} =& (a\eta + 2Tx)^T (aTx + D\Omega_7 Cx + T\dot{x}) \\ & - (Tx)^T (aTx + D\Omega_7 Cx). \end{aligned} \tag{22}$$

If the input is chosen so that

$$T\dot{x} = -(a\eta + 2Tx) - aTx - D\Omega_7 Cx \tag{23}$$

then

$$\begin{aligned} \dot{W} =& -(a\eta + 2Tx)^T (a\eta + 2Tx) \\ & - (Tx)^T (aTx + D\Omega_7 Cx) \end{aligned} \tag{24}$$

or

$$\begin{aligned} \dot{W} =& -(a\eta + 2Tx)^T (a\eta + 2Tx) \\ & - a(Tx)^T Tx - x^T C^T \Delta_7^2 \Omega_7 Cx. \end{aligned} \tag{25}$$

Taking into account that $\Delta_7^2 \Omega_7$ is antisymmetric, which eliminates the last term, the derivative may finally be expressed as

$$\dot{W} = -(a\eta + 2Tx)^T (a\eta + 2Tx) - a(Tx)^T Tx \tag{26}$$

which states that this derivative is negative definite ($\dot{W} < 0$) if $a > 0$, indicating a closed-loop system with global asymptotic stability.

1) Closed-Loop Dynamics: The closed-loop dynamics are then given by the control law definition

$$T\dot{x} = -a\eta - (a+2)Tx - D\Omega_7 Cx \tag{27}$$

or

$$\begin{cases} T\dot{x} = -(a+2)Tx - a\eta - D\Omega_7 Cx \\ \dot{\eta} = Tx \end{cases} \tag{28}$$

or, introducing $\Lambda_1^2 = (a+2)I_7$

$$\begin{cases} \dot{x} = -T^+ \Lambda_1^2 Tx - aT^+ \eta - C^T \Omega_7 Cx \\ \dot{\eta} = Tx \end{cases}. \tag{29}$$

The positive scalar a is a tuning parameter.

2) Control Law: The control law is deduced from

$$\begin{aligned} \dot{x} &= Kx + M^{-1}(ESa_g + f) \\ &= -T^+ \Lambda_1^2 Tx - aT^+ \eta - C^T \Omega_7 Cx \end{aligned} \tag{30}$$

leading to

$$f = M\left(-T^+ \Lambda_1^2 Tx - aT^+ \eta - C^T \Omega_7 Cx - Kx\right) - ESa_g \tag{31}$$

or

$$f = -MT^T \Delta_7^{-2}\left(a\eta + \Lambda_1^2 Tx\right) - M(C^T \Omega_7 C + K)x - ESa_g. \tag{32}$$

III. Saturation Definition and Properties

In order to cope with limitations due to the unmodeled aerodynamic forces or to reduced actuation, it is important to investigate the possibility of introducing saturations into the control design. The definitions presented hereafter are inspired on the definitions introduced by Teel [17] and allow to extend the stability of the control solution presented above.

Definition 1: As a particular case and extension of the linear saturation definition proposed by Teel, let us introduce the element-wise nondecreasing saturation function $\sigma : \mathbb{R}^n \rightarrow \mathbb{R}^n$, defined by a vector m of n positive values m_i, with $R > m_i > r > 0$, and such that

$$\forall z, \sigma[z] = \Sigma z \tag{33}$$

where the diagonal matrix Σ is defined by

$$\begin{aligned} |z_i| < m_i &\Rightarrow \Sigma_i = 1 \\ |z_i| \geq m_i &\Rightarrow \Sigma_i = \frac{m_i}{|z_i|}. \end{aligned} \tag{34}$$

Properties: It may be easily verified that the definition yields the following properties [17]:

$$\begin{cases} \forall z, z^T \sigma[z] > 0 \\ \forall z, |\sigma[z]| \leq R \\ |z| < r \Rightarrow \sigma[z] = z \end{cases} \tag{35}$$

where $|z| = \sqrt{z^T z}$ is the norm of vector z as defined in $\mathbb{R}^n$ and $R^2 = \sum_j m_j^2$.

Theorem 1: If $z^T v = 0$, then

$$z^T \sigma[z + v] > 0. \tag{36}$$

Proof: Since v is orthogonal to z, it may be expressed as $v = \Omega z$, where Ω is antisymmetric, and we then have

$$z^T \sigma[z + v] = z^T \Sigma (z + \Omega z) = z^T \Sigma z + z^T \Sigma \Omega z. \tag{37}$$

Considering the last term and since it is a scalar, we have

$$z^T \Sigma \Omega z = (z^T \Sigma \Omega z)^T = -z^T \Omega \Sigma z \tag{38}$$

and then

$$z^T \Sigma (z + \Omega z) = \frac{1}{2} z^T \left(\Sigma (I + \Omega) + (I - \Omega) \Sigma \right) z \tag{39}$$

or

$$z^T \Sigma (z + \Omega z) = z^T X z \tag{40}$$

where X is a symmetric matrix with a positive diagonal, which leads to the presented result. ∎

Theorem 2: If two saturations σ_1 and σ_2 are defined, such that $R_1 < (1/2) r_2$, then

$$\forall (z_1, z_2), |z_2| > \frac{1}{2} r_2 \Rightarrow z_2^T \sigma_2 \left[z_2 + \sigma_1[z_1] \right] > 0. \tag{41}$$

Proof: Since $|z_2| > (1/2) r_2$ and $|\sigma_1[z]| \leq R_1 < (1/2) r_2$, the orthogonal projection of the saturated vector on z_2 may be expressed as

$$\sigma_1[z_1] = \lambda_1 z_2 + v_1 \tag{42}$$

where $|\lambda_1| < 1$, $z_2^T v_1 = 0$, and $|\lambda_1 z_2 + v_1| < (1/2) r_2$, leading to

$$|z_2 + \lambda_1 z_2 + v_1| < r_2 \tag{43}$$

and then

$$\begin{aligned} z_2^T \sigma_2 \left[z_2 + \sigma_1[z_1] \right] &= z_2^T \sigma_2 \left[(1 + \lambda_1) z_2 + v_1 \right] \\ &= z_2^T \Sigma \left((1 + \lambda_1) z_2 + v_1 \right) \\ &= (1 + \lambda_1) z_2^T \Sigma z_2 > 0. \end{aligned} \tag{44}$$

∎

Corollary: If $|z_2| > (1/2) r_2$ and $|\sigma_1[z]| < (1/2) r_2$, and $z_2^T v_2 = 0$, then

$$z_2^T \sigma_2 \left[z_2 + v_2 + \sigma_1[z_1] \right] > 0. \tag{45}$$

Proof: If

$$\sigma_1[z_1] = \lambda_1 z_2 + v_1 \tag{46}$$

then

$$z_2^T \sigma_2 \left[z_2 + v_2 + \sigma_1[z_1] \right] = z_2^T \sigma_2 \left[(1 + \lambda_1) z_2 + v_2 + v_1 \right] \tag{47}$$

which may be written as

$$(1 + \lambda_1) z_2^T \sigma_2 [z_2 + v] \tag{48}$$

which, using theorem 1 and $|\lambda_1| < 1$, leads to the desired result. ∎

Theorem 3: If $\lambda_1 > 1$, then for all $|z_2| < |z_1|$

$$(z_2 + z_1)^T (z_2 + \lambda_1 z_1) > 0. \tag{49}$$

Proof: Since $|z_2| < |z_1|$, the orthogonal projection of z_2 on z_1 gives

$$z_2 = \lambda_2 z_1 + v_2 \tag{50}$$

where $|\lambda_2| < 1$ and $v_2^T z_1 = 0$, leading to

$$\begin{aligned} (z_2 + z_1)^T (z_2 + \lambda_1 z_1) &= \left((\lambda_2 + \lambda_1) z_1 + v_2 \right)^T \\ &\quad \times \left((\lambda_2 + 1) z_1 + v_2 \right) \\ &= (\lambda_2 + \lambda_1)(\lambda_2 + 1) z_1^T z_1 + v_2^T v_2 \\ &> 0. \end{aligned} \tag{51}$$

∎

IV. Control Saturation

In order to include the input limitations into the design phase, the control law (32) is adapted with the inclusion of satura-

tions in the feedback law according to the definitions introduced above.

Let us first recall the control input obtained previously [(32)]. This can be written as

$$f = -MA^T(Ax + \Gamma x + B\eta) - ESa_g \tag{52}$$

where

$$\begin{aligned} A &= \Delta_7^{-1}\Lambda_1 T \\ B &= a\Delta_7^{-1}\Lambda_1^{-1}\Lambda \\ \Gamma &= \Lambda_1^{-1}\Delta_7^{-1}T(C^T\Omega_7 C + K). \end{aligned} \tag{53}$$

By introducing saturation functions σ_1 and σ_2, respectively, on $B\eta$ and Ax, we obtain the saturated forces input

$$f_s = -MA^T\sigma_2\left[Ax + \Gamma x + \sigma_1[B\eta]\right] - ESa_g. \tag{54}$$

Looking for the stability of the velocity state, let us define $W_2 = (1/2)x^Tx$. Considering the saturated force input f_s, the velocity derivative is

$$\dot{x} = Kx + M^{-1}(ESa_g + f_s) \tag{55}$$

$$\dot{x} = Kx - A^T\sigma_2\left[Ax + \Gamma x + \sigma_1[B\eta]\right] \tag{56}$$

leading to

$$\dot{W}_2 = x^TKx - x^TA^T\sigma_2\left[Ax + \Gamma x + \sigma_1[B\eta]\right]. \tag{57}$$

The first term is zero since K is antisymmetric and, introducing $z_1 = B\eta$, $z_2 = Ax$ and $v_2 = \Gamma x$, the equation may be written as

$$\dot{W}_2 = -z_2^T\sigma_2\left[z_2 + v_2 + \sigma_1[z_1]\right]. \tag{58}$$

If the saturations are chosen so that $R_1 < (1/2)r_2$, then, using theorem 2 and its corollary, it may be deduced that, for $|z_2| > (1/2)r_2$, $\dot{W}_2 < 0$, showing that W_2 is a Lyapunov function, and thus, after a finite time T_2, the variable z_2 will enter the linear zone of its saturation and remain in it.

After time T_2, the force input is then

$$f_s = -MA^T\left(Ax + \Gamma x + \sigma_1[B\eta]\right) - ESa_g \tag{59}$$

and the velocity derivative is

$$\dot{x} = Kx - A^T\left(Ax + \Gamma x + \sigma_1[B\eta]\right) \tag{60}$$

or

$$\dot{x} = -A^T\left(Ax + \sigma_1[B\eta]\right) - C^T\Omega_7 Cx. \tag{61}$$

Recalling now the overall function $W = (1/2)y_1^Ty_1 + (1/2)y_2^Ty_2$, of which the derivative (22) is

$$\dot{W} = (a\eta + 2Tx)^T(aTx + D\Omega_7 Cx + T\dot{x}) - a(Tx)^T(Tx) \tag{62}$$

introducing the corrected velocity derivative yields

$$\dot{W} = -(a\eta + 2Tx)^T\Delta_7\Lambda_1\left(2\Delta_7^{-1}Ax + \sigma_1[B\eta]\right) - a(Tx)^T(Tx) \tag{63}$$

or

$$\dot{W} = -(B\eta + 2Ax)^T\Delta_7^2\Lambda_1^2\Lambda^{-1}(2Ax + \sigma_1[B\eta]) - a(Tx)^T(Tx) \tag{64}$$

or even

$$\dot{W} = -(X_2z_2 + X_1z_1)^T\left(X_2z_2 + X_1\sigma_1[z_1]\right) - a(Tx)^T(Tx) \tag{65}$$

with

$$\begin{aligned} X_2 &= 2\Delta_7\Lambda_1^{-1} = 2(a+2)^{-1/2}\Delta_7 \\ X_1 &= \Delta_7\Lambda_1 = (a+2)^{1/2}\Delta_7. \end{aligned} \tag{66}$$

From the above formulas, and considering that all of the design parameters are positive, it may be verified that both X_1 and X_2 are positive diagonal matrices and that their minimum and maximum eigenvalues verify

$$\lambda_{max}(X_2) < 2^{1/2} < \lambda_{min}(X_1) \tag{67}$$

which leads to

$$|z_2| < |\sigma_1[z_1]| \Rightarrow |X_2z_2| < |X_1\sigma_1[z_1]|. \tag{68}$$

Then, if $|\sigma_1[z_1]| \geq r_1$, using theorem 3 shows that $\dot{W} < 0$, and otherwise, in the linear region, $\sigma_1[z_1] = z_1$. Clearly, we also have $\dot{W} < 0$, finally showing the exponential stability of the controlled system.

V. Application to an Airship UAV

The proposed backstepping controller is valid for a generic UAV in near-hover conditions. However, the assumptions made in the design, namely, neglecting the aerodynamic forces, are more or less legitimate depending on the type of UAV considered. In the airship hovering case, for instance, the nonmodeling of the aerodynamic forces is a rough approximation due to the airship big volume when compared, for instance, with the helicopter case. Hence, to implement the proposed approach for the hovering stabilization of an airship UAV in the presence of wind disturbances represents a real challenge to the controller performance and robustness.

To justify the controller applicability on different UAV types, we will not consider actuators inputs, since they are highly platform-dependent. However, and in order to have meaningful forces saturations, it is necessary to know the application UAV actuators and how they are related with input forces.

In the sequel, the case of the Autonomous Unmanned Remote mOnitoring Robotic Airship (AURORA) Project AS800B airship [22] will be considered.

A. Airship Actuators

The AURORA airship actuators list (see Fig. 1) may be split into the following two sets.

1) Force inputs are available from the vectored two main propellers, on each side of the gondola, providing a complementary lift to oppose the weighting mass, as well as a forward thrust controlling the longitudinal speed. When a differential input is added between the two propellers,

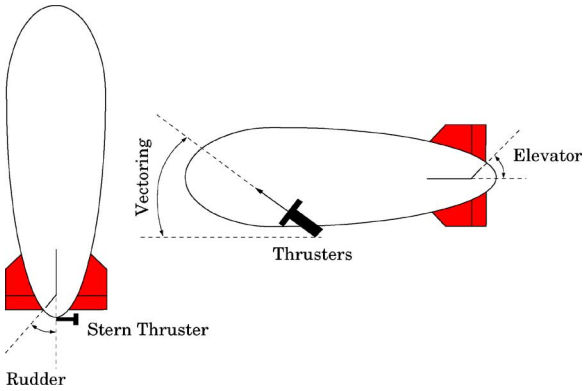

Fig. 1. Airship actuators.

they also provide torque to control the rolling motion near hover. Finally, a stern lateral thruster may be necessary to provide yaw control at low airspeeds, but it has not been used in the AURORA airship standard configuration.

2) Surface deflections of the tail, in the presence of a minimum airspeed provide torque inputs mostly for the control of the pitching and yawing motions.

When the air is perfectly still and there is no wind incidence, the hover control is reduced to the use of only the first set.

B. Airship Forces

Although the real airship is commanded by the actuators' action, forces will be used as input in the simulation environment in order to directly test the proposed controller. However, based in the knowledge of the real airship actuators and their bounds, saturations on the control input corresponding to absolute force/torque maxima were obtained

$$\begin{aligned} |f_1| &< 107\ \text{N} \\ |f_2| &< 13\ \text{N} \\ |f_3| &< 40\ \text{N} \\ |f_4| &< 27\ \text{N}\cdot\text{m} \\ |f_5| &< 267\ \text{N}\cdot\text{m} \\ |f_6| &< 27\ \text{N}\cdot\text{m}. \end{aligned} \tag{69}$$

The observation of the above limits clearly indicates a higher control amplitude over the longitudinal motion than over the lateral one, as expected.

C. Dealing With the Lateral Sub-Actuation

If the objective is hovering with respect to the ground or a ground target, the wind disturbance appears both as:

- a positive factor, which will help to control the airship thanks to the increased authority of the tail control surfaces;
- a drawback, producing a mostly horizontal force that needs to be balanced by an airship actuator. This is only possible using the longitudinal forces and aligning the airship to reduce the drag force.

As a consequence, and in order to avoid the saturation occurrences resulting from the reduced lateral controllability, along with the definition of suitable saturation limits, it is necessary to correct the control objective. In the presence of wind, the wind heading provides a nonarbitrary yaw reference. This way, the airship may align itself against the wind, and the lateral force input may vanish in stationary conditions. However, to do so the wind heading must be available. This value may be estimated using the measurement of the airship velocity, as well as airspeed V_t and sideslip angle β.

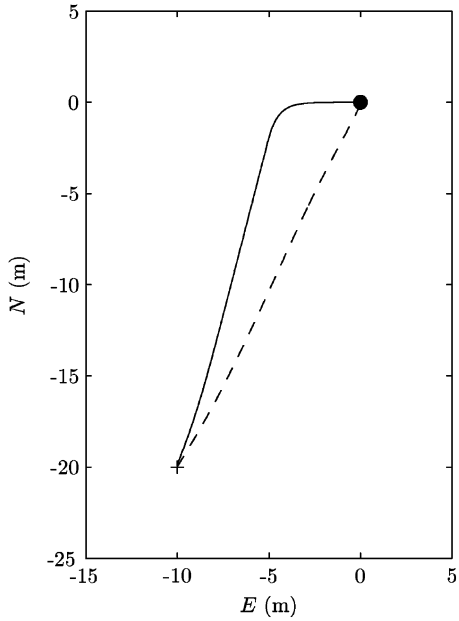

Fig. 2. Horizontal path, in full forces case (dashed line) and saturated case (solid line).

D. Simulation Results

With the purpose of evaluating the design approach, repetitive simulation tests were performed under MATLAB/Simulink, using the fully nonlinear platform developed in the AURORA project [22], to reproduce the motion of an airship prototype weighting 33 kg and with a volume of 30 m^3.

All results presented here concern the hover stabilization of the airship at constant altitude. For illustrative purposes, in examples A and B the attitude of the airship is initially set out of equilibrium, with 10° in all Euler angles.

The aerodynamic forces were neglected during the controller design, however they are obviously present in any real flight. Moreover, the influence of wind disturbances must be considered, whether still wind or even turbulent gust. Therefore, results from three different scenarios are presented next.

1) Example A: The first example compares two situations starting from initial coordinates $(N_i, E_i) = (-20, -10)\text{m}$, the first with full forces (dashed line) and the second considering saturation limits (solid line), both with no wind incidence.

Fig. 2 shows the horizontal North-East path, and Fig. 3 shows the position variables: the cartesian coordinates and the Euler angles (the attitude is here presented in terms of the Euler angles—see Fig. 4—which are more meaningful and intuitive than the quaternions).

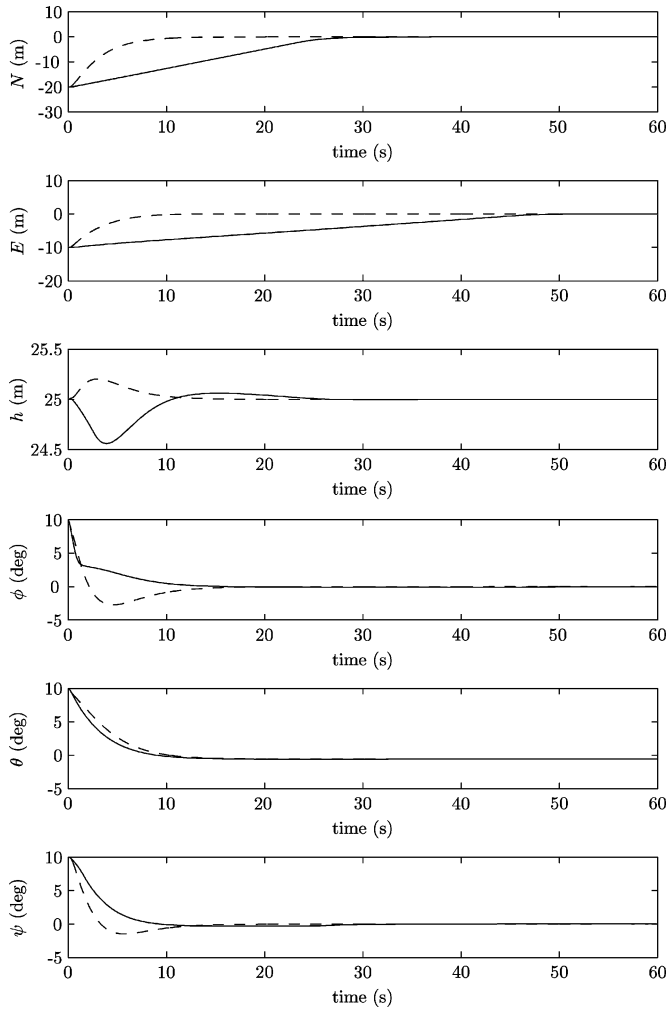

Fig. 3. Position variables, in full forces case (dashed line) and saturated case (solid line) and from top to bottom, the cartesian North-East-Up coordinates, and roll-pitch-yaw Euler angles.

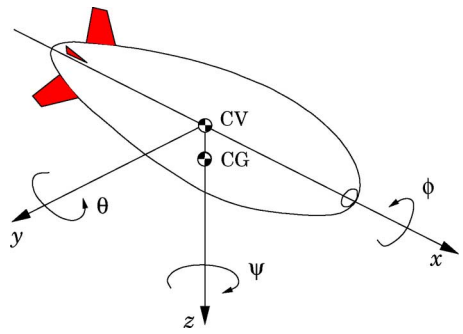

Fig. 4. Euler angles definition in local frame.

In both cases, the airship is perfectly taken to its reference position. The full forces case is obviously faster, with Cartesian position and attitude stabilized between 10 and 15 s, whereas the saturated case needs around 15 to 50 s to reach the stable state. The saturation effect is perfectly visible on the North and East time curves, where the full forces case is typical of a first order response and the saturated curves exhibit a constant time rate, which is a direct consequence of the input saturation. Furthermore, the saturation has a lower limit for the lateral force

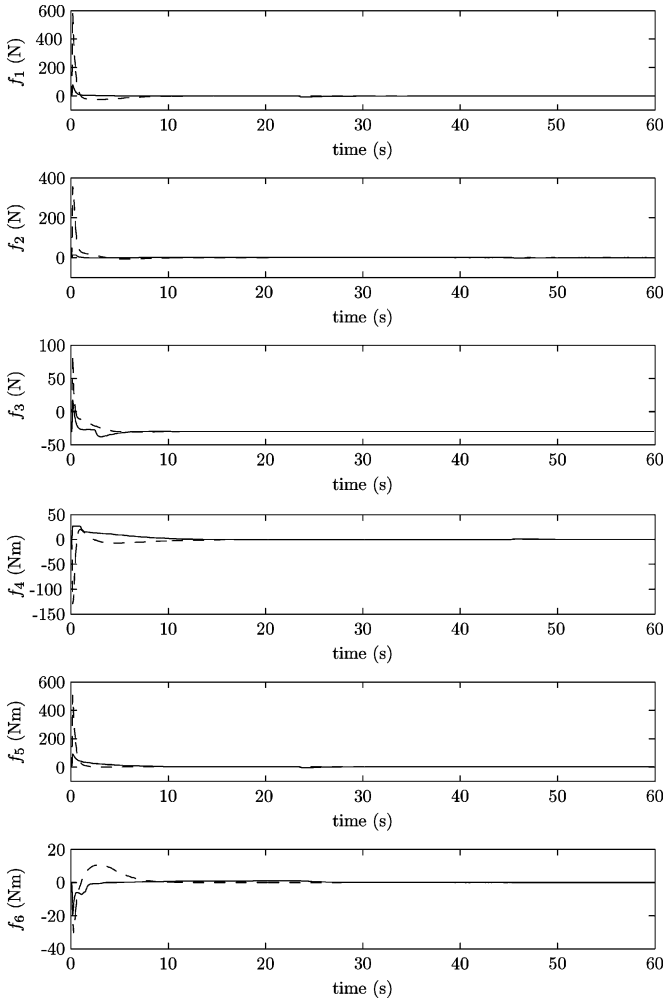

Fig. 5. Control inputs, with full actuation (dashed line) and saturated case (solid line), forces on top and torques below.

$(f_{2_{\max}} = 13\,\mathrm{N})$ than for the longitudinal one $(f_{1_{\max}} = 107\,\mathrm{N})$, resulting in a quicker longitudinal positioning, which explains the final lateral correction visible in the horizontal path curve. The altitude h control is also worth of notice, exhibiting a good regulation, with an error below 50 cm in both cases. As for the attitude, the three Euler angles, roll, pitch and yaw (ϕ, θ, ψ) are in both cases rapidly corrected.

The control inputs are shown in Fig. 5, with the force (f_1, f_2, f_3) time curves on top and the torque (f_4, f_5, f_6) curves below. The initial peak forces and torques of the full actuation case go over 600 N and 500 Nm, reducing then to much smaller values during the rest of the simulation. In order to have a better analysis of the saturation effect, a zoom of the previous figure is presented in Fig. 6, with the initial 10 s only. The saturation limits are clearly visible for the lateral force f_2 and the rolling torque f_4, for instance.

The airspeed time curves are presented in Fig. 7, depicting the airship velocity until stabilization is achieved. In this no-wind case, the airspeed is obviously equal to the airship velocity measured relatively to the ground. The full forces case (dashed line) presents an airspeed with a short settling time, around 10 s, but the airspeed climbs up to around 5.5 m/s, a value for which the aerodynamic forces are already significative. These forces

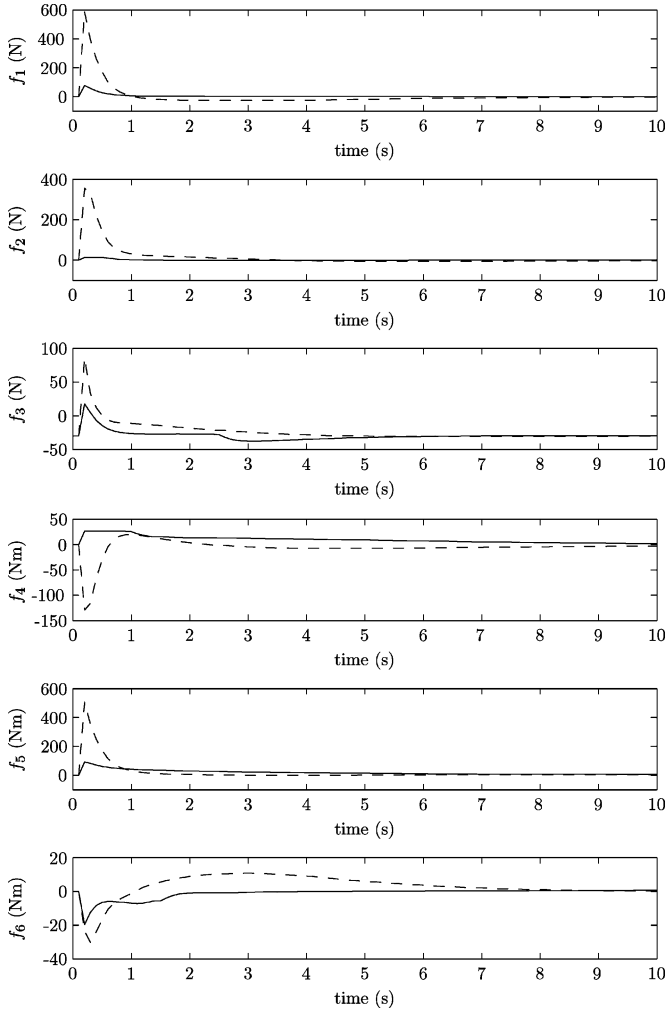

Fig. 6. Control inputs curves zoom, with full actuation (dashed line) and saturated case (solid line), forces on top and torques below.

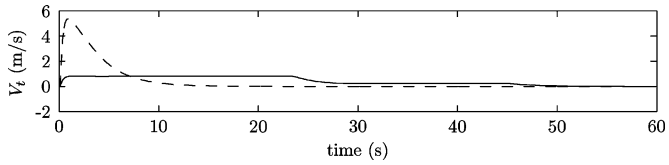

Fig. 7. Airspeed, for full forces case (dashed line) and saturated case (solid line).

were neglected for the control design but are obviously present in the simulation. The controller is however perfectly robust to this disturbance. In the saturated case (solid line), the airspeed climbs only to 0.8 m/s, and in this case the disturbance is reduced. In both cases the aerodynamics is clearly under control and the interference with the positioning objective (see Figs. 2 and 3) is small (namely, this explains why the full forces horizontal path is not a perfect straight segment).

2) Example B: The second example considers the saturated forces case only. Here, 8 trajectories from different North–East initial conditions are compared, considering a constant 3-m/s wind blowing from North.

Fig. 8 shows the horizontal North–East path, and Fig. 9 shows the position variables formed by the Cartesian coordinates and

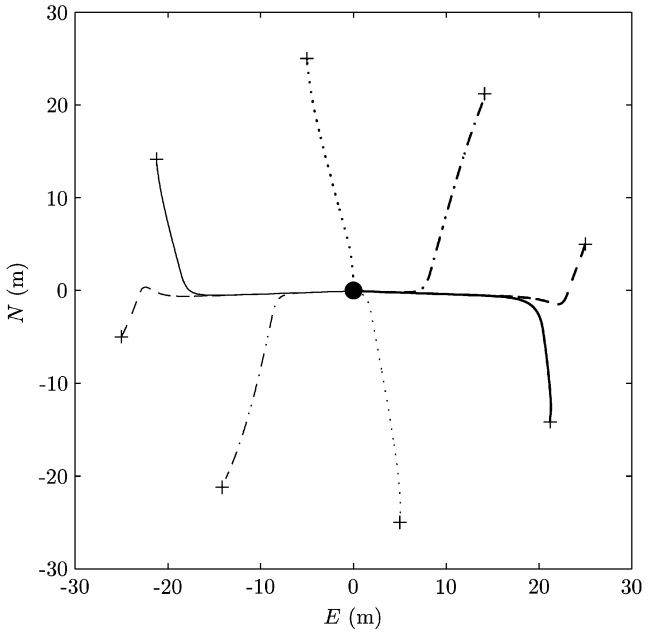

Fig. 8. Horizontal path for different starting points, for saturated forces case.

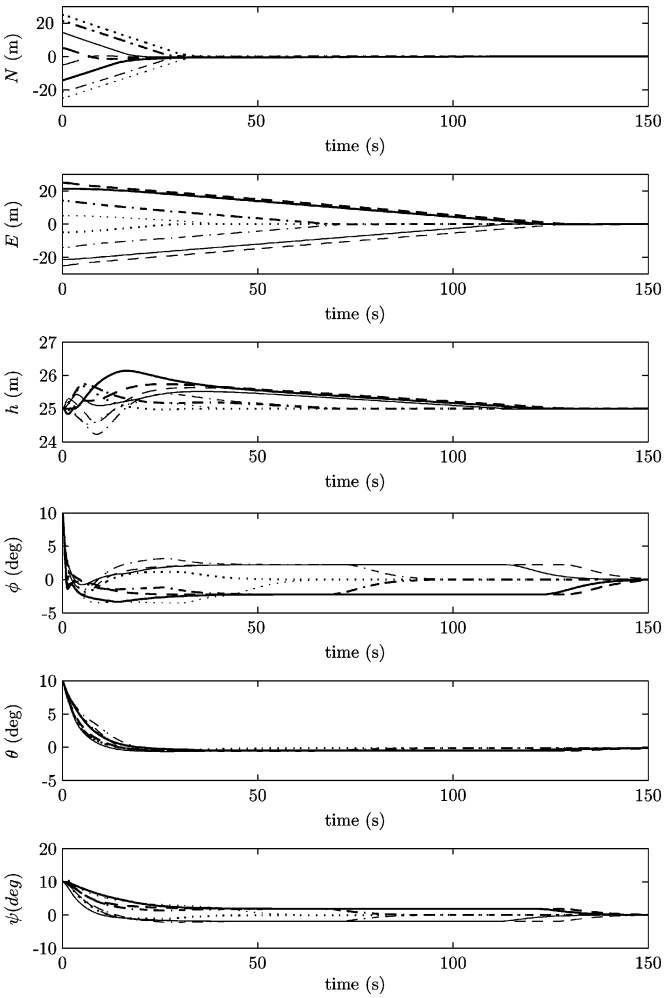

Fig. 9. Position variables for different starting points, for saturated forces case.

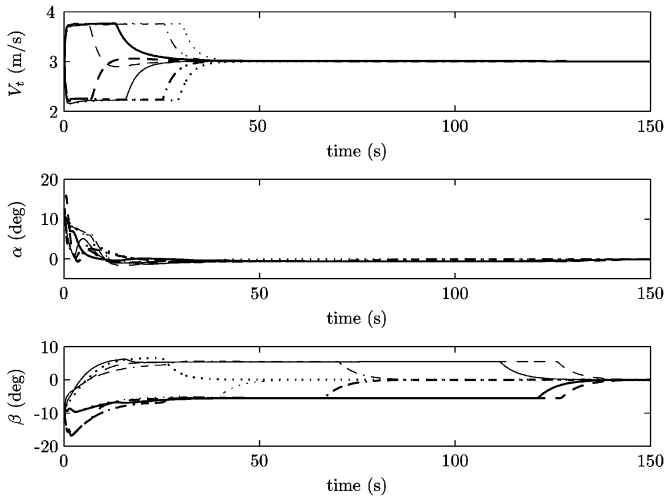

Fig. 10. Airspeed and aerodynamic angles for different starting points, for saturated forces case.

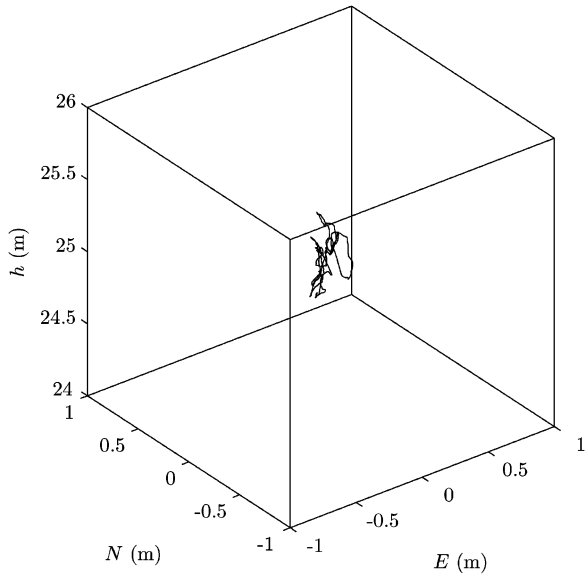

Fig. 11. Airship 3-D position coordinates for turbulent gust case.

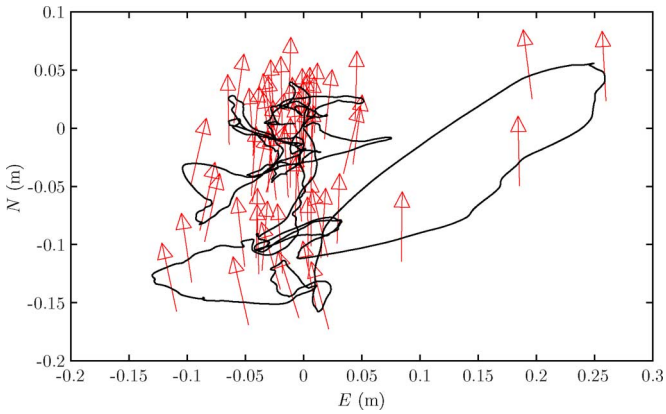

Fig. 12. Horizontal path with airship yaw angle for turbulent gust case.

the Euler angles. In all cases the airship is perfectly taken to its reference position.

With the exception of the altitude, the stabilization of the longitudinal variables (N, θ) in about 35 s is much faster than the almost 150 s necessary for the lateral ones (E, ϕ, ψ) to reach the stable state. This is result of the airship lateral forces restrictions. Once again, the saturation effect is perfectly visible on the North and East time curves which exhibit a constant time rate, a direct consequence of the input saturation. Moreover, as referred to in example A, the saturation has a lower limit for the lateral force than for the longitudinal one resulting in a quicker longitudinal positioning, which explains the final lateral correction visible in the horizontal path curves. The altitude h control again exhibits a good regulation, with an error almost always below 1 m.

In order to better evaluate the influence of the aerodynamic forces, the airspeed time curves are presented in Fig. 10, along with the two aerodynamic angles, α and β. Remember that a constant 3-m/s wind speed is blowing from North, and so the stable airspeed is also equal to 3 m/s and the stable values for the angles are zero. In all cases, the airspeed magnitude is below 0.8 m/s (positive or negative depending if the airship had to go against or with the wind to achieve the reference position) representing a reduced disturbance. In all cases the aerodynamics is clearly under control and the interference with the positioning objective (see Figs. 8 and 9) is small.

A symmetry is visible between the curves on opposite sides, result of the symmetry of the initial conditions provided.

3) Example C: The third example considers the saturated forces case with a 3-m/s North constant wind, and in addition a 3-m/s turbulent gust. The turbulence is modeled in the simulation platform using a continuous gust Dryden model [23]. The airship starts at the reference coordinates $(N_{\text{ref}}, E_{\text{ref}}, D_{\text{ref}}) = (0, 0, -25)\text{m}$ and with reference attitude $(\phi_{\text{ref}}, \theta_{\text{ref}}, \psi_{\text{ref}}) = (0, 0, 0)\,\text{deg}$. The purpose of this example is to show the controller ability to maintain the airship at the reference position even in the presence of a realistic wind disturbance.

TABLE I
RMS VALUES FOR POSITION VARIABLES AND INPUT FORCES

$N(m)$	$E(m)$	$h(m)$	ϕ(deg)	θ(deg)	ψ(deg)
0.067	0.063	0.179	3.029	2.726	6.412

$f_1(N)$	$f_2(N)$	$f_3(N)$	$f_4(Nm)$	$f_5(Nm)$	$f_6(Nm)$
1.744	3.878	9.764	11.272	8.214	14.844

The airship 3-D position is represented in Fig. 11. With a minor oscillation due to the presence of turbulent gust, the airship is kept within small bounds of the wished position. The North–East-altitude coordinates have an error inferior to 0.2, 0.3, and 0.5 m, respectively. The airship heading shows to be consistent with the prevailing North wind direction, as may be observed in Fig. 12.

The simulation ran during 300 s, after which the rms error of interest variables was computed, in order to have an illustrative quantitative evaluation. The position and input forces rms values are represented in Table I.

The negligible position error values (when compared with the size of the airship) confirm the observation made on Fig. 11. As for the forces, the rms values of f_1 and f_2 indicate a low control

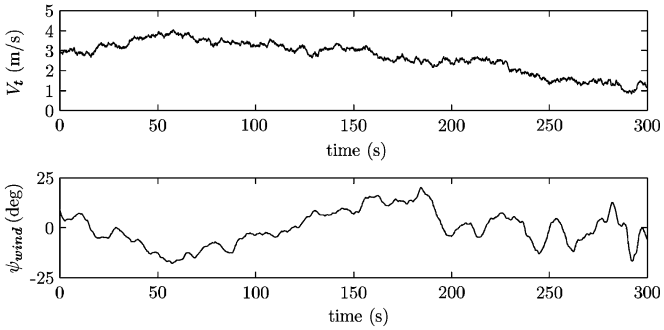

Fig. 13. Airspeed and wind heading estimation for turbulent gust case.

effort of the N and E variables, which in fact have the lowest error values. A higher control effort is requested of f_4, f_5 and f_6 to maintain the attitude variables stable, more sensitive to the presence of wind disturbances.

As opposed to example B, in this case the wind heading is not constant owed to the incidence of turbulent gust. The estimation of the wind heading made during the simulation is important in order to provide an attainable yaw reference to the airship. Fig. 13 depicts the airspeed and wind heading estimation. The significant variation of both variables can be noticed (V_t varies between 1 and 4 m/s and ψ_{wind} between -20 and 20 deg), as well as the relatively high frequency of both signals, both of which are results of the turbulent gust.

In this case, the aerodynamic forces undoubtedly play an important role. However, the controller has no knowledge of these forces and thus provides no direct action to compensate then. Even so, the results obtained illustrate a good controller robustness to the existence of such realistic wind disturbances.

VI. Conclusion

This brief introduced a synthetic dynamic model for a generic UAV, valid for quasi-stationary conditions, with quaternion formulation of the kinematics equations. A backstepping design formulation based in this model was then deduced for UAV hover control and its global asymptotic stability demonstrated. In order to cope with limitations due to reduced actuation, saturations were introduced in the control design, and the stability of the modified control solution verified.

The proposed solution was based on a generic UAV model that considers forces and torques as inputs and the AURORA airship simulation platform was adapted for the purpose. However, UAVs are known to be commanded through the action of actuators like rotors or control surfaces. In order to straightforwardly apply the proposed control solution, the actuators limitations were converted into force constraints. The inclusion of the real actuators as inputs is the obvious subsequent step. However, such a step is highly platform-dependent, and the approach is to be carefully adapted according to the UAV characteristics.

Although some assumptions made during the controller design might, at a first glance, exclude its application for the hover stabilization of an airship UAV, simulation results show the excellent performance of the proposed controller on such lighter-than-air UAVs. Also, its robustness in the face of wind disturbances, which represent a major concern for the specific case of airships, show that this is a highly promising approach. The implementation on the AURORA flying prototype is currently under development.

References

[1] D. Grace, M. Mohorcic, M. Oodo, M. H. Capstick, M. B. Pallavicini, and M. Lalovic, "CAPANINA communications from aerial platform networks delivering broadband information for all," presented at the IST Mobile Wireless Summit, Dresden, Germany, Jun. 2005.

[2] L. Merino, F. Caballero, J. R. M. de Dios, and A. Ollero, "Cooperative fire detection using unmanned aerial vehicles," in *Proc. IEEE Int. Conf. Robot. Autom.*, Apr. 2005, pp. 1884–1889.

[3] J. R. Azinheira, P. Rives, J. R. H. Carvalho, G. F. Silveira, E. C. de Paiva, and S. S. Bueno, "Visual servo control for the hovering of an outdoor robotic airship," in *Proc. IEEE Int. Conf. Robot. Autom.*, Washington, DC, May 2002, pp. 2787–2792.

[4] H. Shim, T. J. Koo, F. Hoffmann, and S. Sastry, "A comprehensive study of control design for an autonomous helicopter," in *Proc. 37th IEEE Conf. Decision Control*, Tampa, FL, Dec. 1998, pp. 3653–3658.

[5] L. Guo, C. Melhuish, and Q. Zhu, "Towards neural adaptive hovering control of helicopters," in *Proc. IEEE Int. Conf. Control Applications*, Glasgow, U.K., Sep. 2002, pp. 54–58.

[6] C.-D. Yang and W.-H. Liu, "Nonlinear h_∞ decoupling hover control of helicopter with parameter uncertainties," in *Proc. Amer. Control Conf.*, Denver, CO, Jun. 2003, pp. 3454–3459.

[7] R. Mahony, T. Hamel, and A. Dzul, "Hover control via Lyapunov control for an autonomous model helicopter," in *Proc. 38th Conf. Decision Control*, Dec. 1999, vol. 4, pp. 3490–3495.

[8] F. Lin, W. Zhang, and R. D. Brandt, "Robust hovering control of a PVTOL aircraft," *IEEE Trans. Control Syst. Technol.*, vol. 7, no. 3, pp. 343–351, May 1999.

[9] N. Metni, T. Hamel, and F. Derkx, "A UAV for bridge's inspection: Visual servoing control law with orientation limits," presented at the 5th IFAC/EURON Symp. Intell. Auton. Vehicles, Lisbon, Portugal, Jul. 2004.

[10] T. J. Koo and S. Sastry, "Output tracking control design of a helicopter model based on approximate linearization," in *Proc. 37th IEEE Conf. Decision Control*, Tampa, FL, 1998, pp. 3635–3640.

[11] H. K. Khalil, *Nonlinear Systems*, 3rd ed. Upper Saddle River, NJ: Prentice-Hall, 2000.

[12] K.-S. Kim and Y. Kim, "Robust backstepping control for slew maneuver using nonlinear tracking function," *IEEE Trans. Control Syst. Technol.*, vol. 11, no. 6, pp. 822–829, Nov. 2003.

[13] E. Hygounenc and P. Soueres, "Automatic airship control involving backstepping techniques," presented at the IEEE Int. Conf. Syst., Man Cybern., Hammamet, Tunisia, Oct. 2002.

[14] E. Frazzoli, M. A. Dahleh, and E. Feron, "Trajectory tracking control design for autonomous helicopters using a backstepping algorithm," in *Proc. Amer. Control Conf.*, Chicago, IL, Jun. 2000, pp. 4102–4107.

[15] L. Beji, A. Abichou, and Y. Bestaoui, "Stabilization of a nonlinear underactuated autonomous airship—A combined averaging and backstepping approach," in *Proc. 3rd Int. Workshop Robot Motion Control*, Bukowy Dworek, Poland, Nov. 2002, pp. 223–229.

[16] G. J. Toussaint, T. Basar, and F. Bullo, "Tracking for nonlinear underactuated surface vessels with generalized forces," in *Proc. IEEE Int. Conf. Control Applicat.*, Anchorage, AK, Sep. 2000, pp. 355–360.

[17] A. R. Teel, "Global stabilization and restricted tracking for multiple integrators with bounded controls," *Syst. Control Lett.*, vol. 18, no. 3, pp. 165–171, Mar. 1992.

[18] R. Freeman and L. Praly, "Integrator backstepping for bounded controls and control rates," *IEEE Trans. Autom. Control*, vol. 43, no. 2, pp. 258–262, Feb. 1998.

[19] J. R. Azinheira, E. C. de Paiva, and S. S. Bueno, "Influence of wind speed on airship dynamics," *J. Guid., Control, Dynam.*, vol. 25, no. 6, pp. 1116–1124, Nov.–Dec. 2002.

[20] X. Deng, L. Schenato, and S. Sastry, "Hovering flight control of a micromechanical flying insect," in *Proc. 40th IEEE Conf. Decision Control*, Dec. 2001, vol. 1, pp. 235–240.

[21] B. L. Stevens and F. L. Lewis, *Aircraft Control and Simulation*. New York: Wiley, 1992.

[22] E. C. de Paiva, J. R. Azinheira, J. Josué, G. Ramos, A. Moutinho, and S. S. Bueno, "Project AURORA: Infrastructure and flight control experiments for a robotic airship," *J. Field Robot.*, vol. 23, no. 3/4, pp. 201–222, Mar./Apr. 2006.

[23] D. McLean, *Automatic Flight Control Systems*. Englewood Cliffs, NJ: Prentice-Hall, 1990.